Electronic Supplementary Information

Niobium and tantalum complexes derived from the acids $Ph_2C(X)CO_2H$ (X = OH, NH_2): Synthesis, structure and ROP capability

Xin Zhang, Timothy J. Prior and Carl Redshaw*

Plastics Collaboratory, Department of Chemistry, The University of Hull, Cottingham Rd, Hull HU6 7RX, United Kingdom.

Contents

Figure S14. Plot of relationship between conversion and time (min) for the polymerization of *r*-LA (Table 2, entry 5-8).

Figure S15. 2D homo *J*-resolved NMR ($CDCl_3$, 400 MHz) of PLA (Table 2, entry 5).

Figure S16. 2D homo *J*-resolved NMR ($CDCl_3$, 400 MHz) of PLA (Table 2, entry 6).

Figure S17. 2D homo *J*-resolved NMR ($CDCl_3$, 400 MHz) of PLA (Table 2, entry 7).

Figure S18. 2D homo *J*-resolved NMR ($CDCl_3$, 400 MHz) of PLA (Table 2, entry 8).

Figure S19. 2D homo *J*-resolved NMR ($CDCl_3$, 400 MHz) of PLA (Table 2, entry 9).

Figure S20. 2D homo *J*-resolved NMR ($CDCl_3$, 400 MHz) of PLA (Table 2, entry 10).

Figure S21. 2D homo *J*-resolved NMR ($CDCl_3$, 400 MHz) of PLA (Table 2, entry 11).

Figure S22. 2D homo *J*-resolved NMR ($CDCl_3$, 400 MHz) of PLA (Table 2, entry 12).

Figure S23. ^1H NMR ($CDCl_3$, 400 MHz) of PDLLA-*b*-CL (Table 3, entry 3).

Figure S24. ^1H NMR ($CDCl_3$, 400 MHz) of the intensity of methylene protons for CL-LA and CL-CL (Table 3, entry 6).

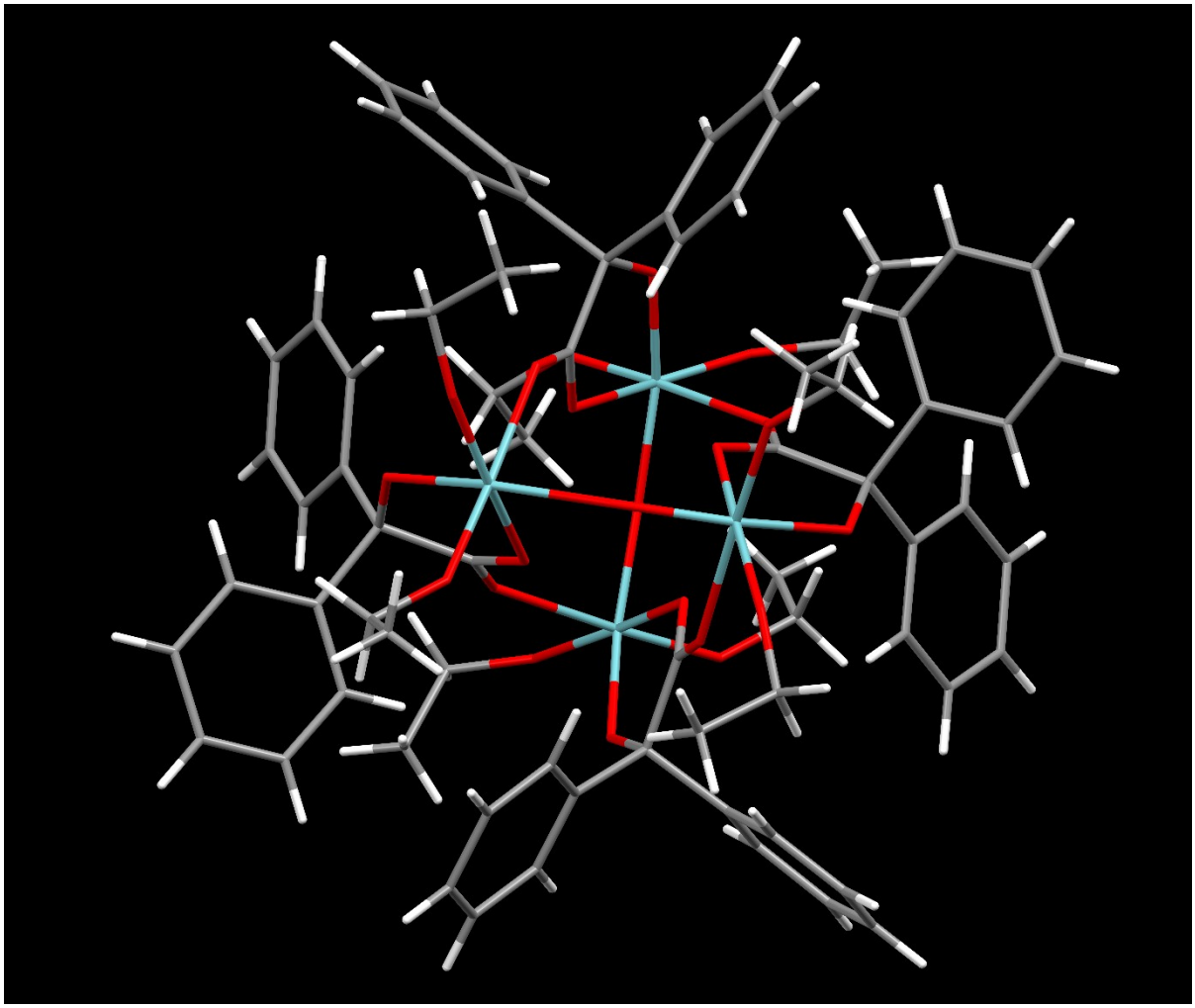

Figure S1. Alternative view of four niobium cluster present in **1**.

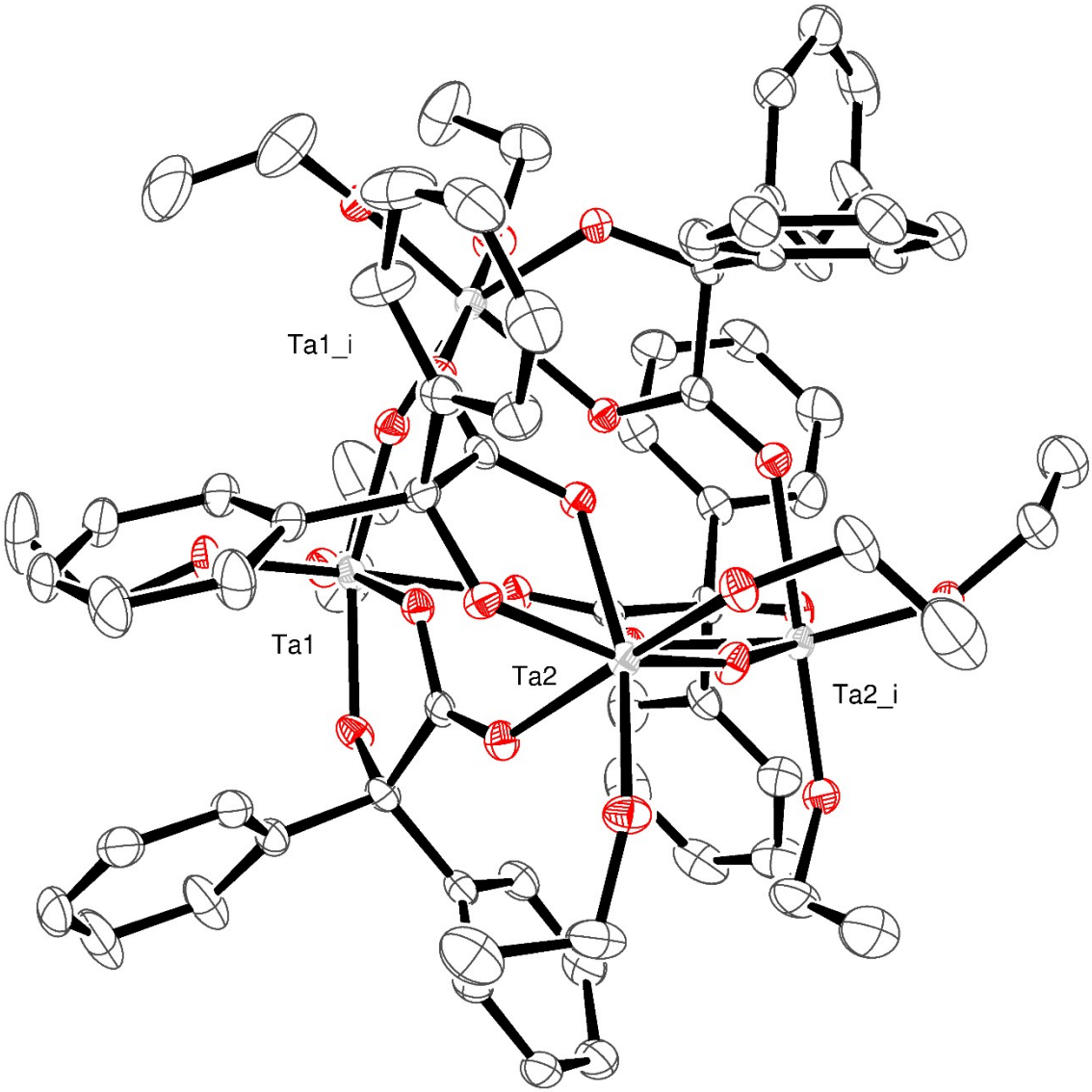

Figure S2. Alternative view of the four-tantalum cluster present in **2·0.5MeCN**. Atoms are drawn as 50% probability ellipsoids. Symmetry operation: i = 1−x, y, ½ −z.

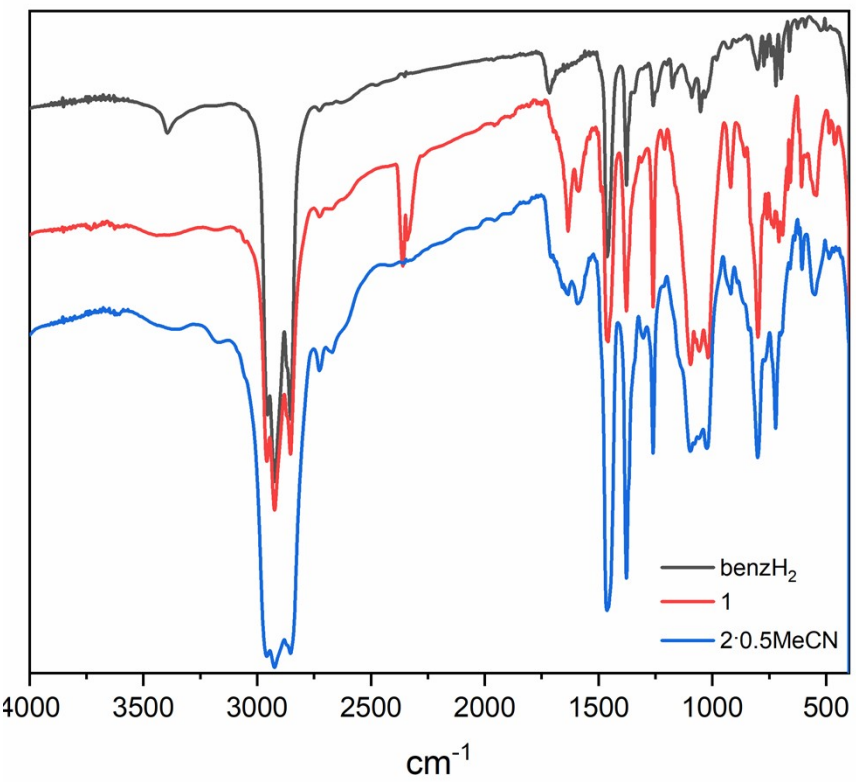

Figure S3. IR spectrum of L^1H_2, **1** and **2**·0.5MeCN in nujol.

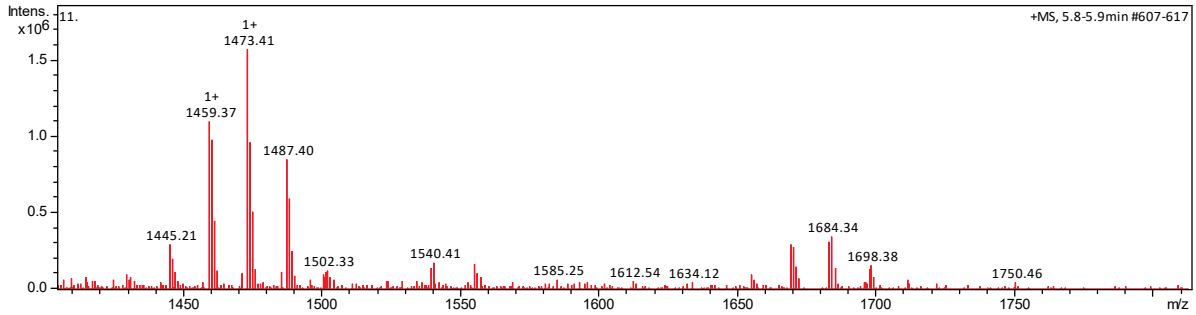

Figure S4. ESI-MS spectrum of **1**.

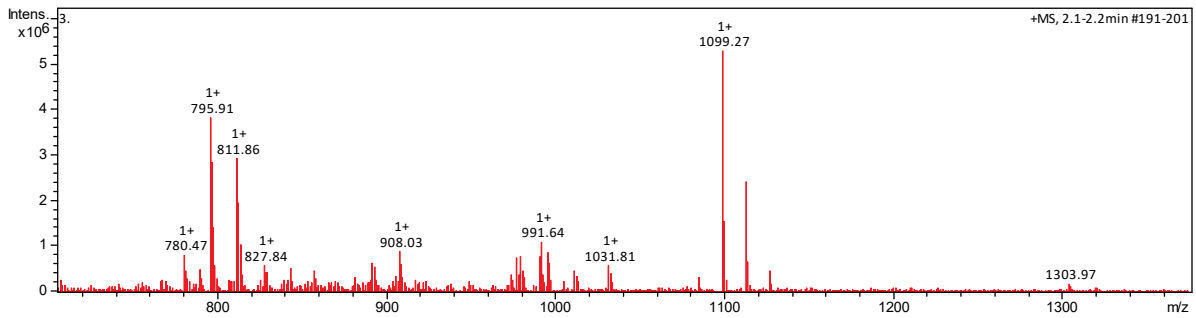

Figure S5. ESI-MS spectrum of **2**·0.5MeCN.

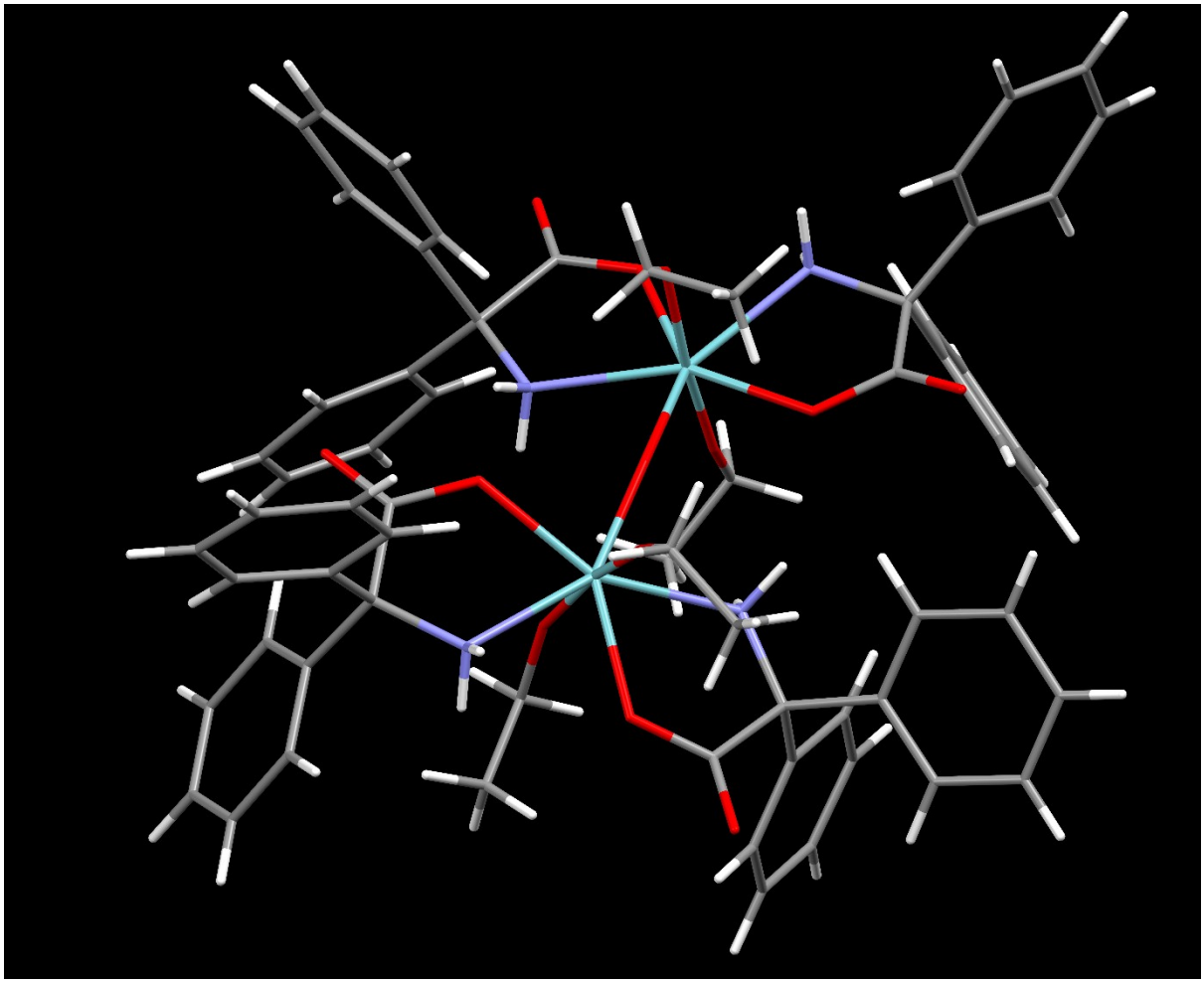

Figure S6. Alternative view of the asymmetric unit of **3**·2MeCN

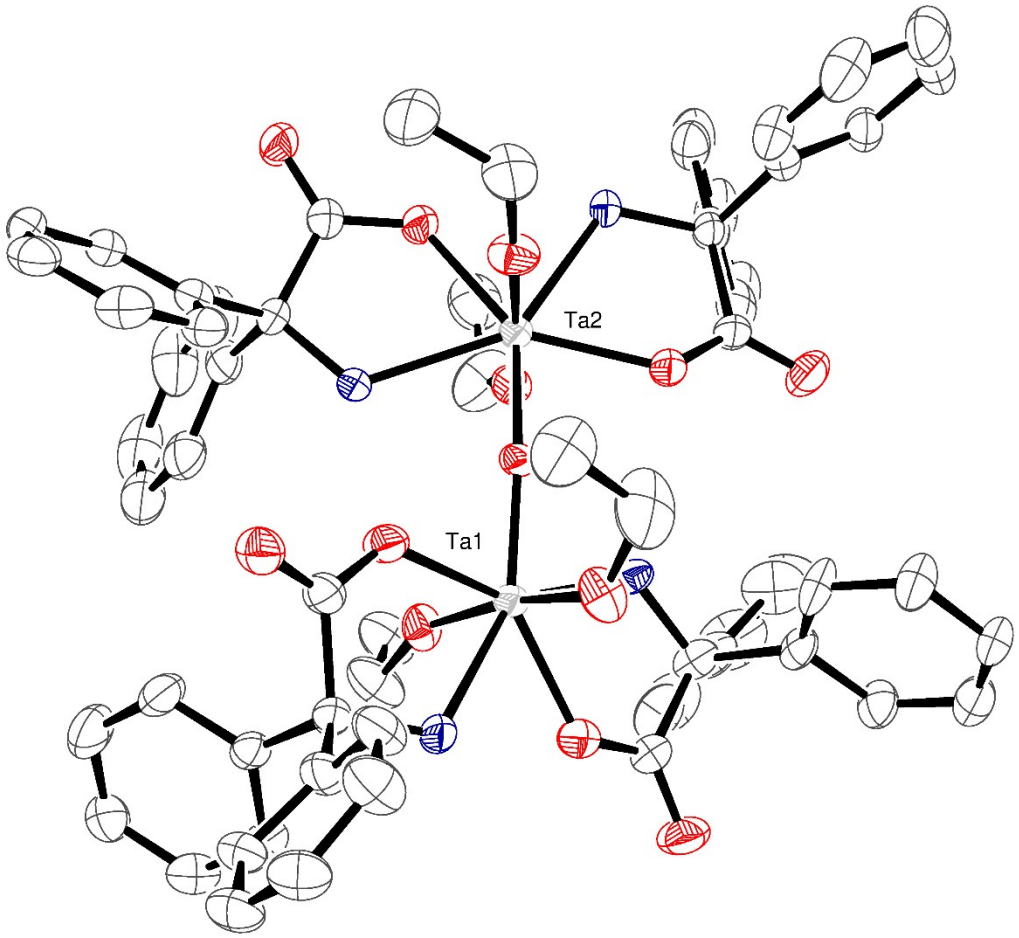

Figure S7. Asymmetric unit of **4**·2.25MeCN with atoms drawn as 50% probability ellipsoids.

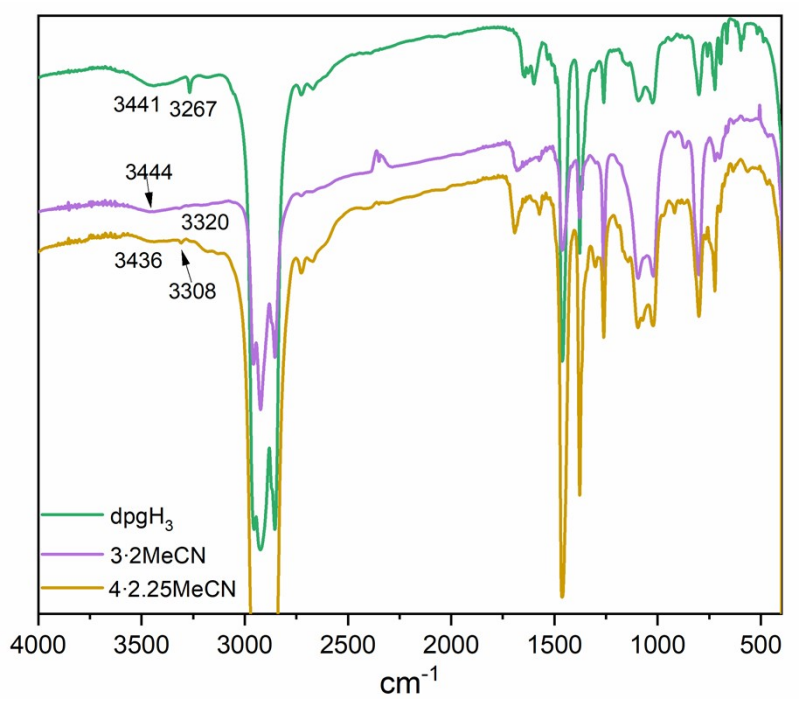

Figure S8. IR spectrum of L^2H_3, **3**·2MeCN and **4**·2.25MeCN in nujol.

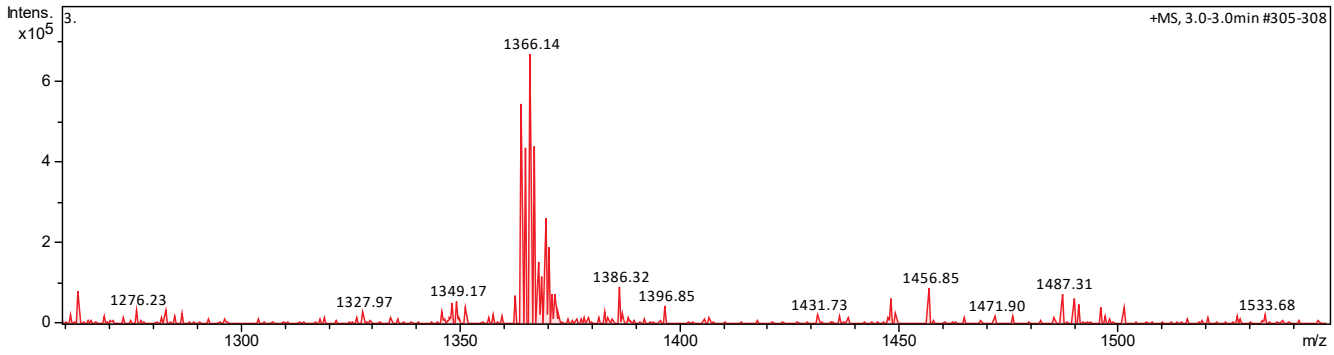

Figure S9. ESI-MS spectrum of **3**·2MeCN.

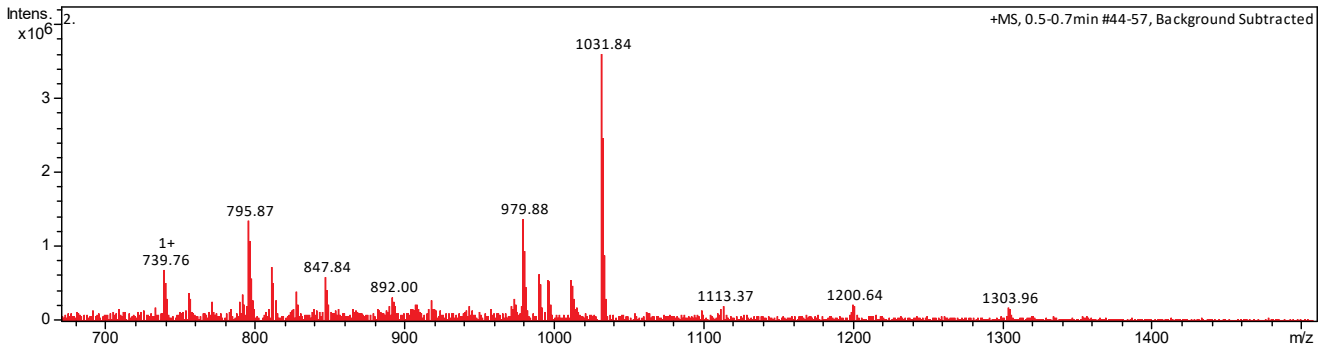

Figure S10. ESI-MS spectrum of **4**·2.25MeCN.

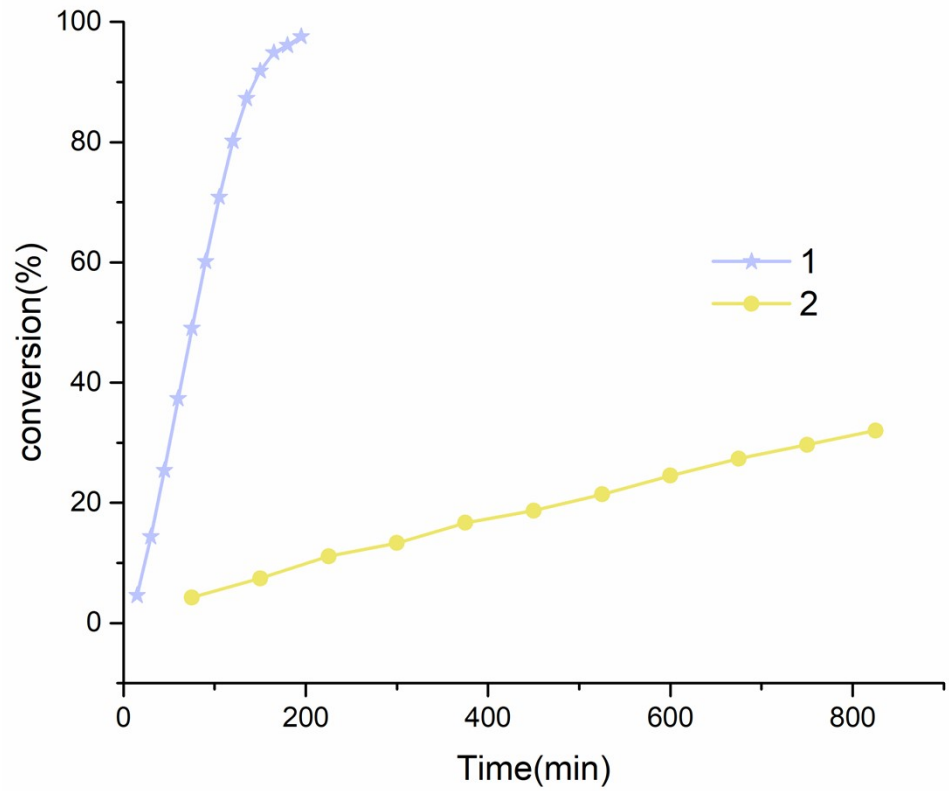

Figure S11. Plot of relationship between conversion and time (min) for the polymerization of ε-CL (Table 1, entry 1-2).

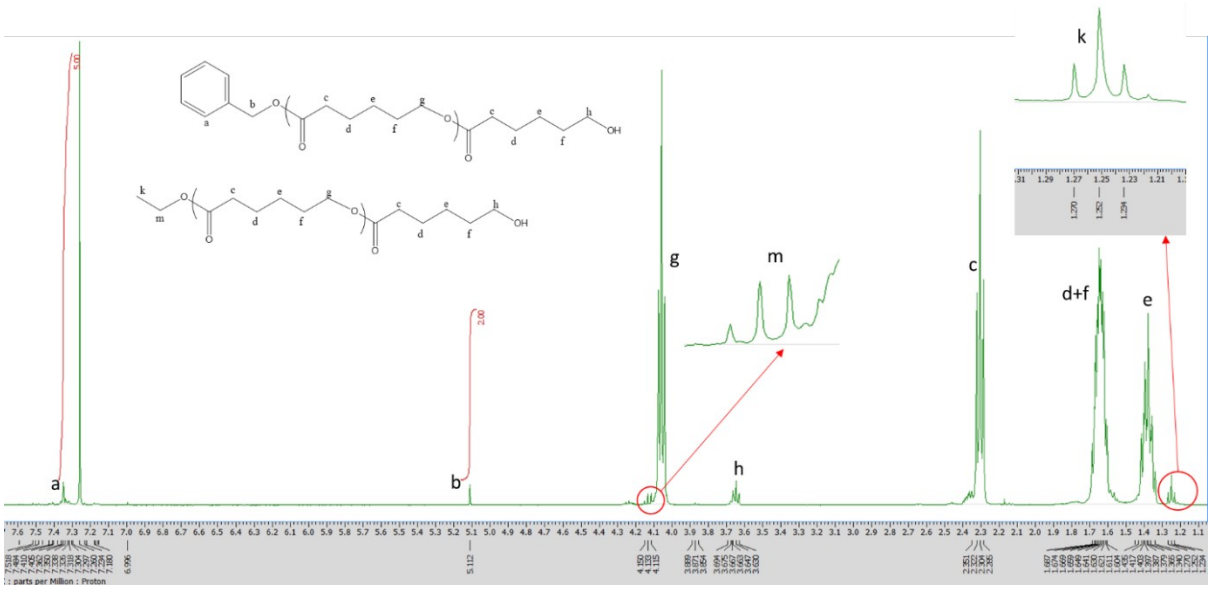

Figure S12. ^{1}H NMR spectrum ($CDCl_3$) of PCL catalyzed by **1** (Table 1, entry 1).

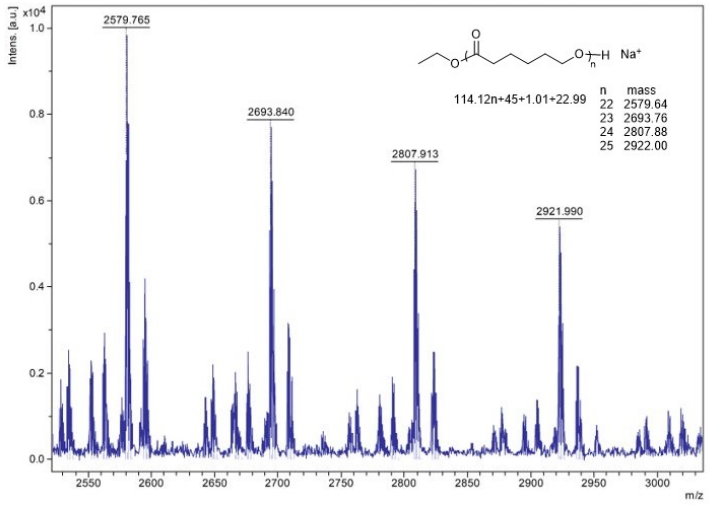

Figure S13. MALDI-TOF spectrum of the PCL catalysed by **1** in the absence of BnOH (Table 1, entry 5); n is the degree of polymerization.

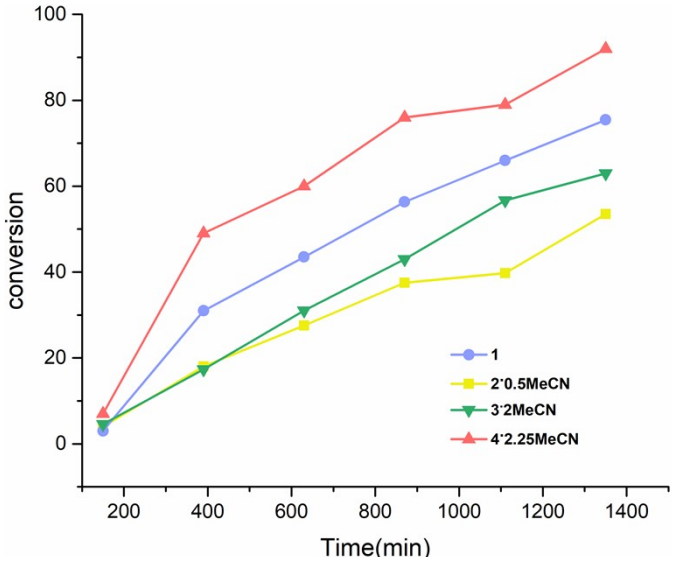

Figure S14. Plot of relationship between conversion and time (min) for the polymerization of *r*-LA (Table 2, entry 5-8).

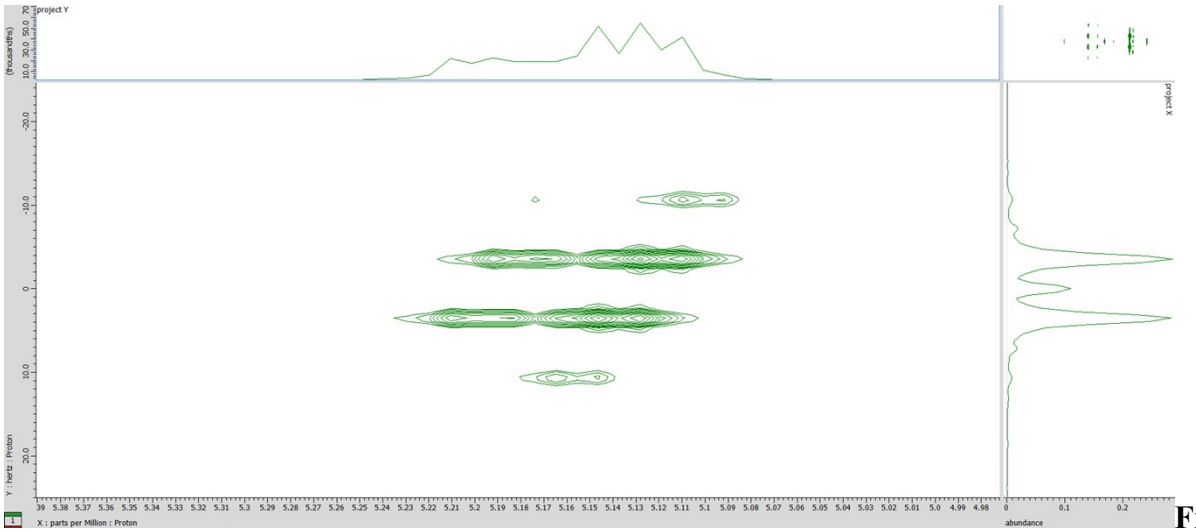

Figure S15. 2D homo *J*-resolved NMR ($CDCl_3$, 400 MHz) of PLA (Table 2, entry 5).

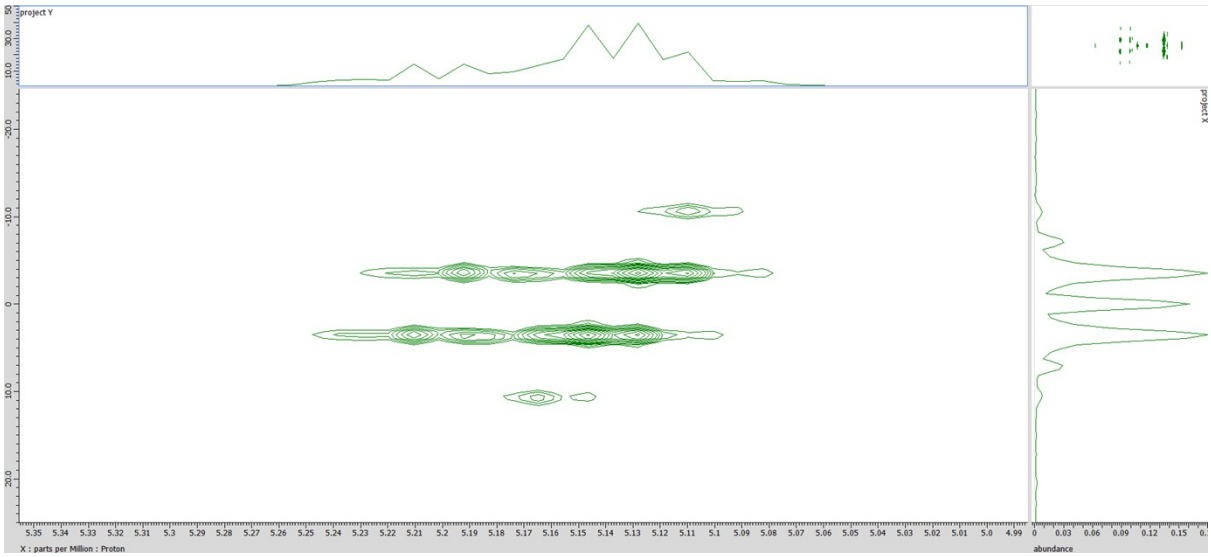

Figure S16. 2D homo *J*-resolved NMR ($CDCl_3$, 400 MHz) of PLA (Table 2, entry 6).

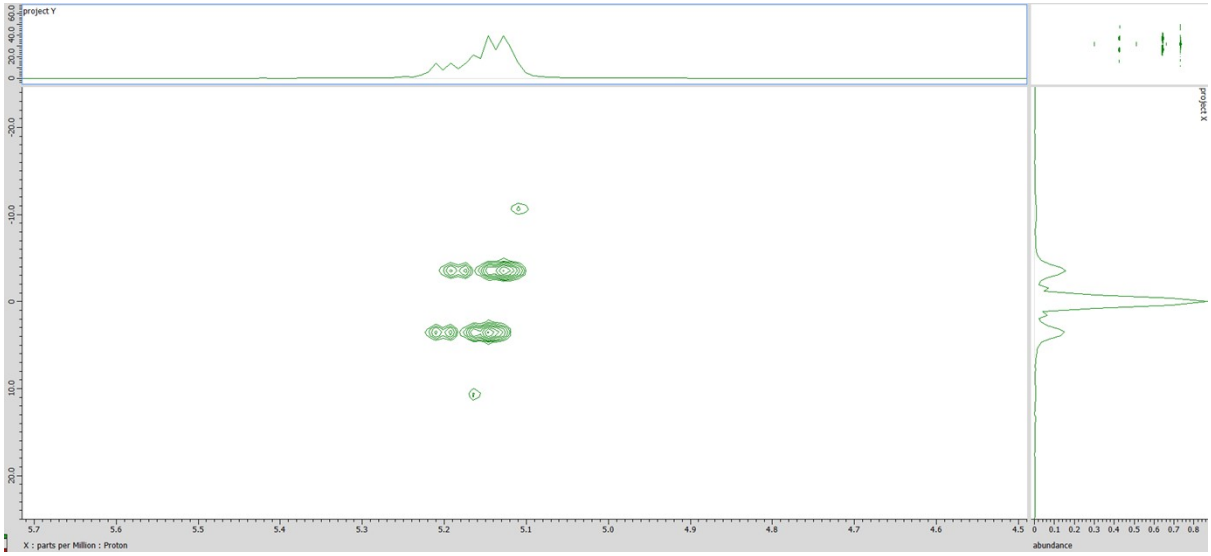

Figure S17. 2D homo *J*-resolved NMR ($CDCl_3$, 400 MHz) of PLA (Table 2, entry 7).

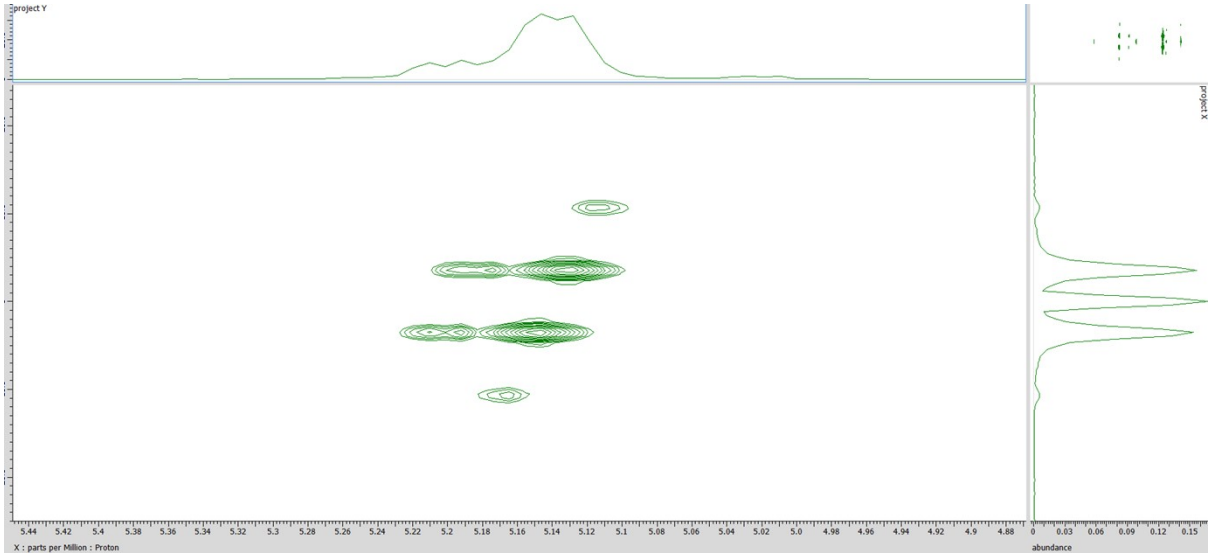

Figure S18. 2D homo *J*-resolved NMR ($CDCl_3$, 400 MHz) of PLA (Table 2, entry 8).

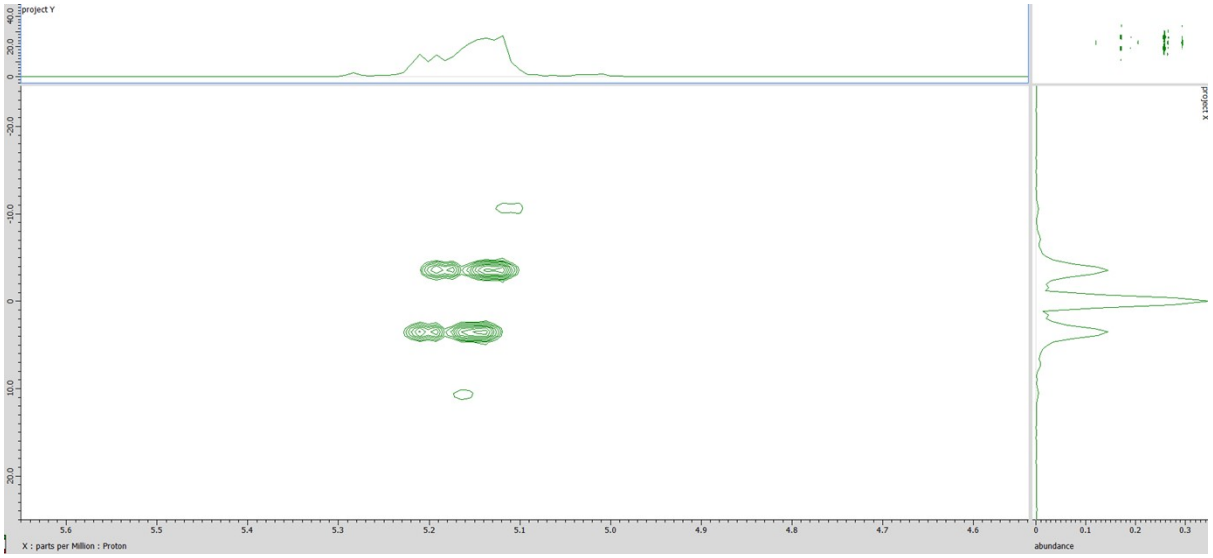

Figure S19. 2D homo *J*-resolved NMR ($CDCl_3$, 400 MHz) of PLA (Table 2, entry 9).

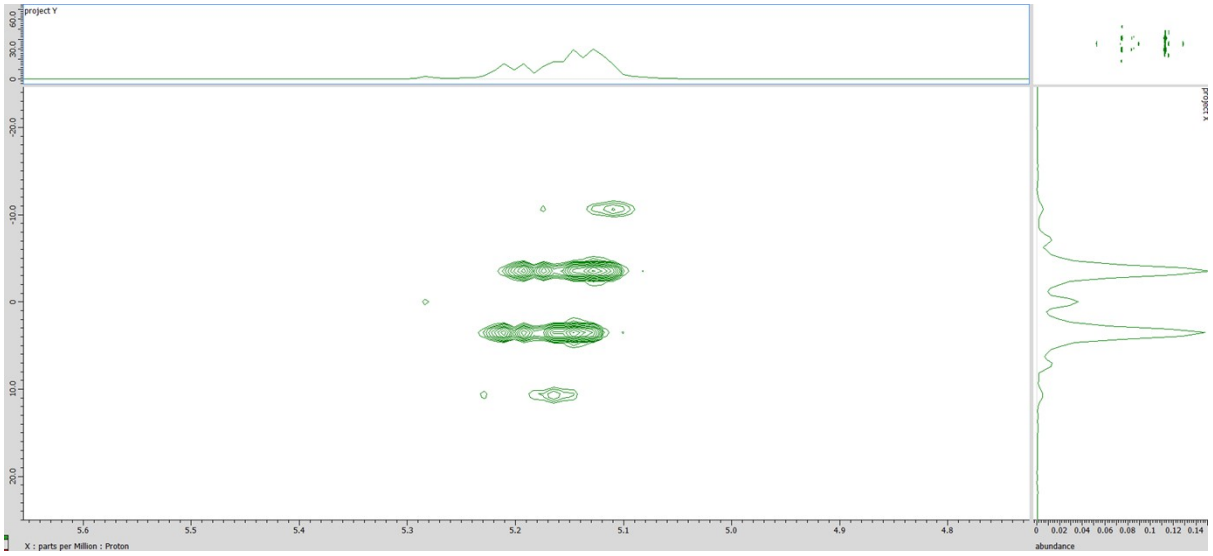

Figure S20. 2D homo *J*-resolved NMR ($CDCl_3$, 400 MHz) of PLA (Table 2, entry 10).

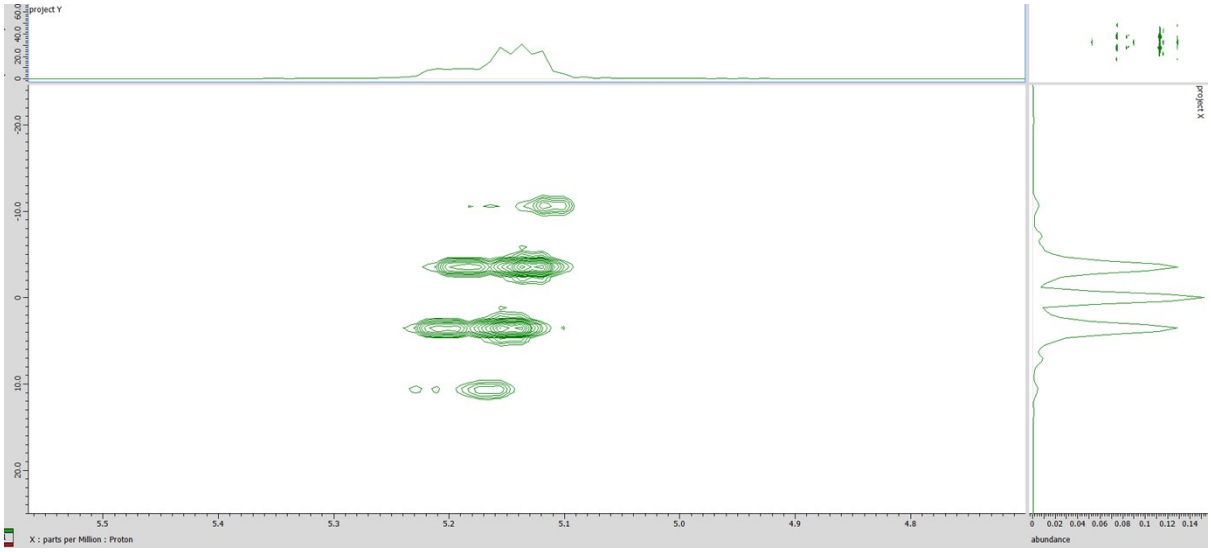

Figure S21. 2D homo *J*-resolved NMR ($CDCl_3$, 400 MHz) of PLA (Table 2, entry 11).

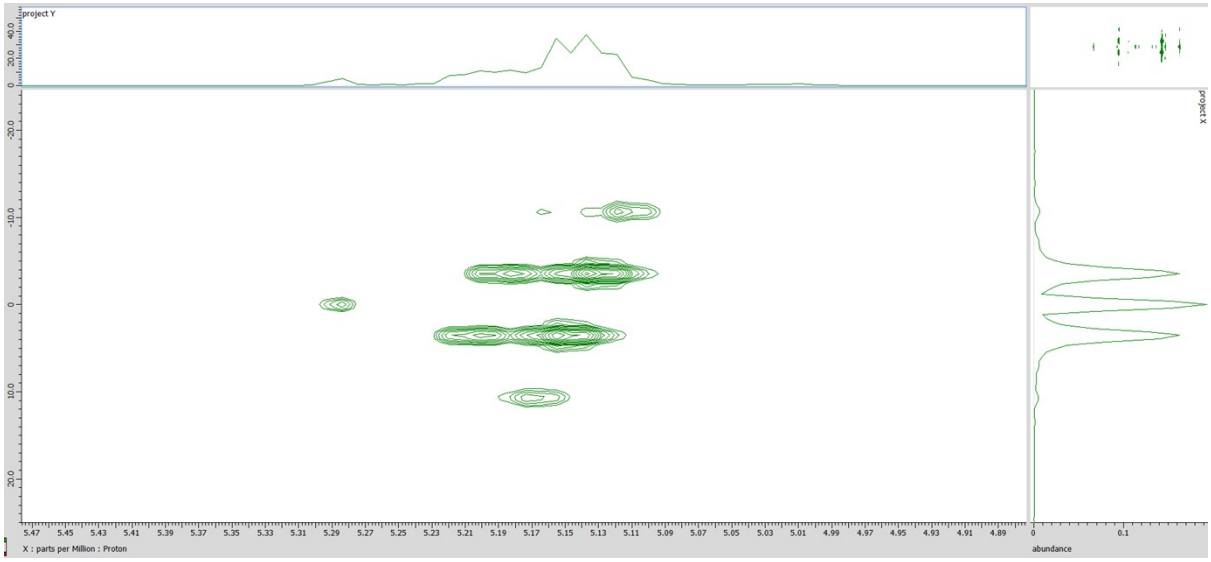

Figure S22. 2D homo *J*-resolved NMR ($CDCl_3$, 400 MHz) of PLA (Table 2, entry 12).

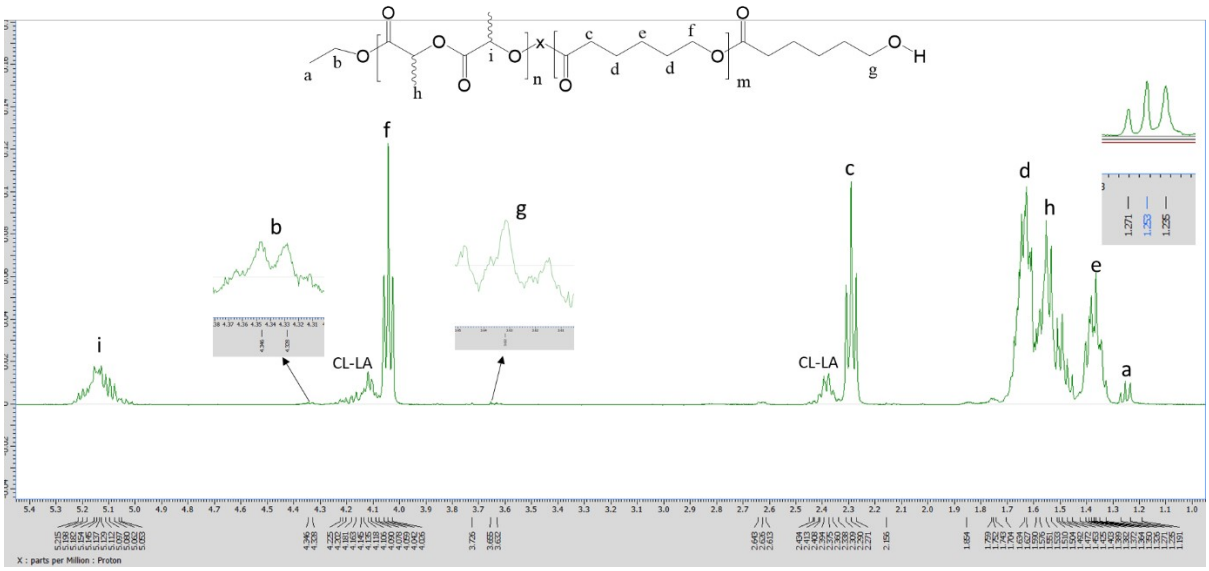

Figure S23. ^{1}H NMR ($CDCl_3$, 400 MHz) of PDLLA-*b*-CL (Table 3, entry 3).

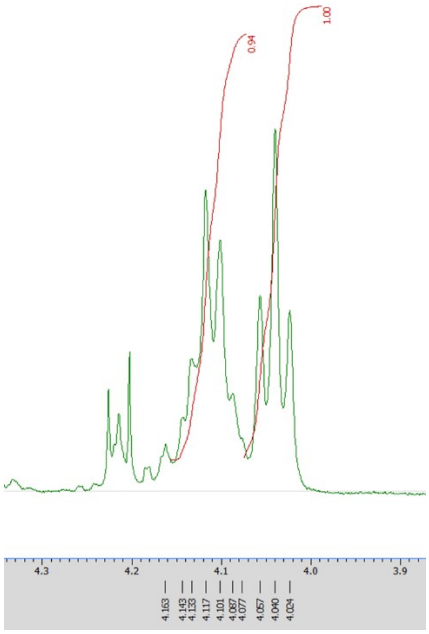

Figure S24. ^{1}H NMR ($CDCl_3$, 400 MHz) of the intensity of methylene protons for CL-LA and CL-CL (Table 3, entry 6).